
ELSEVIER

Infrared Physics & Technology 41 (2000) 361–371

INFRARED PHYSICS & TECHNOLOGY

www.elsevier.com/locate/infrared

High quality infrared (8 μm) diode laser source design for high resolution spectroscopy with precise temperature and current control

D. Weidmann *, D. Courtois

Groupe de Spectrométrie Moléculaire et Atmosphérique, UMR CNRS 6089, Université de Reims Champagne Ardenne, U.F.R. Sciences exactes et naturelles, B.P. 1039, 51687 Reims cedex 2, France

Received 19 June 2000

Abstract

The performance of a tunable diode laser (DL) spectrometer is directly determined by the DL qualities and its tunability control. Emission characteristics are very sensitive to current and temperature drifts. In order to obtain a high quality source for spectroscopy, we designed our own liquid nitrogen cryostat containing the DL. Moreover we compared current and temperature control and we found that temperature tuning can be more efficient. We check and demonstrate it by recording SO_2 spectra in the 1168–1169 cm^{-1} spectral region.

PACS: 42.55.Px; 42.62.Fi
Keywords: High-resolution spectroscopy; Diode laser; Temperature tuning

1. Introduction

Mid infrared tunable diodes laser are a powerful tool for high-resolution absorption spectroscopy [1] and trace gas detection. A diode laser (DL) spectrometer requires the use of a high power source with a narrow linewidth and low intensity noise. This ultimate performance cannot be obtained with multimode emission but only with single mode emission [2]. Indeed, the apparatus function of such a spectrometer is mainly given by the emission linewidth of the DL. Thus, to have the narrowest emission linewidth, we have to set up fine control of the diode temperature and current, which are the two tuning parameters. The spectrometer's resolvance is enhanced by increasing both temperature and current stability.

The development of heterojunction lead salt DLs, emitting in the mid infrared and continuously operating at LN_2 temperature, allows the construction of lighter and less expensive systems than closed cycle cooler or helium evaporation cryostats. Moreover closed cycle coolers induce significant DL emission spectrum broadening [3].

To obtain good temperature stability, we designed a LN_2 cryostat. The temperature control

* Corresponding author. Tel.: +33-3-2691-8311; fax: +33-3-2691-3147.
E-mail address: damien.weidmann@univ-reims.fr (D. Weidmann).

1350-4495/00/$ - see front matter
PII: S1350-4495(00)00055-4

associated with this system is described below. The influence of the current source is also discussed. For testing, we have recorded SO_2 spectra in the region of 1168 cm^{-1}.

2. LN_2 cryostat design

For the design of the DL's cryostat a commercial one has been modified. Fig. 1 shows a view of the system.

The space under the LN_2 tank has been increased. Under the cold plate, we have added a copper bulky cylinder, which plays the role of thermal buffer. An indium foil between the cold plate and the cylinder enhances the thermal contact.

The DL's holder is isolated by a Plexiglass plate (thermal conductivity 0.18 $W m^{-1} K^{-1}$). We took particular care to limit the contact area between the Plexiglass plate and the external metallic shell, to limit the thermal leak.

The DL's holder is made of copper. Near both sides of the DL, two lithographically defined platinum sensors Pt1000 are mounted. We determine the temperature from the DIN 43760 standard calibration curve. Behind the DL, a 15 Ω resistive foil provides the heat supply for temperature regulation.

The thermal link between the buffer and the DL's holder is ensured by a set of 60 copper foils of 25 μm thick. Such a link is flexible and thus the DL's holder is mechanically independent of the LN_2 tank.

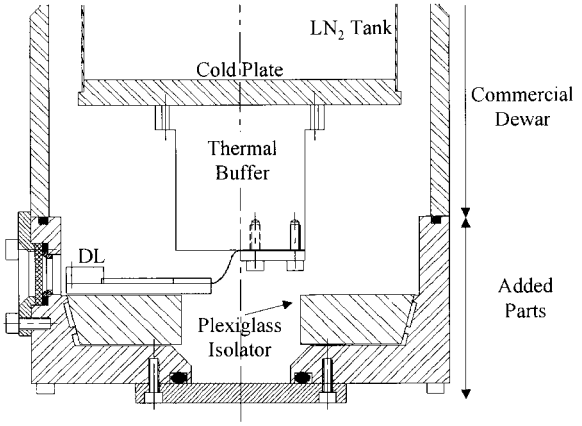

Fig. 1. Schematic view of the DL cryostat.

The DL, the temperature sensors, and the heater are connected via a 12-pin hermetic connector. Usually, the dynamic vacuum in the cryostat is about 5×10^{-6} mbar. Several months use is obtained without re-pumping. The radiation emitted goes through a BaF_2 window.

The low limit temperature reached by the system is 79 K with LN_2 at atmospheric pressure. By pumping above the LN_2, we decrease the LN_2 boiling point and the low-limit temperature falls to 65 K near the triple point of nitrogen. The system has a hold time of 18 h at atmospheric pressure and 12 h when pumping above the LN_2. For our experiments we used a heterojunction lead salt DL (PbSnTe) provided by Laser Photonics.

3. DLs control

3.1. Temperature control

We checked two different temperature controllers, one analog, and the other digital. After testing them, for the experiments presented here, we kept the digital one: the model 340 provided by Lake-Shore. This controller accepts two sensor inputs (with four lead measurements). The sensors excitation current is 1 mA for the Pt1000. Input signals (sensor resistance) are sampled by a 24 bit analog to digital converter; there are 20 measurements per second. The maximum power of the output circuit for the heater is 100 W, the output signal is delivered by an 18 bit digital to analog converter. The controller uses a proportional–integral–derivative algorithm to calculate the feedback. Another very useful feature of the digital controller is its ability to produce a linear ramp of temperature. We will see below the efficiency of this feature.

We need to know the response of the system to adjust the PID characteristics. To determine these parameters, we put the system through a heat step. Then, a thermally thin system model has been used to compute the response time. A system is called

thermally thin when it warms or cools in one piece. Temperature gradients are then negligible. The deciding parameter to validate this hypothesis is the Biot number:

$$\mathrm{Bi} = \frac{hL}{\lambda}, \tag{3.1}$$

where λ is the thermal conductivity, L, the volume of the system divided by its whole exchange surface and h, the thermal exchange coefficient. When $\mathrm{Bi} \ll 1$ the thermally thin model is valid. Here, the system is the DL holder. It is made of copper, so λ is about 400 W $\mathrm{m}^{-1}\,\mathrm{K}^{-1}$. The thermal exchange coefficient h is very small because of the vacuum in the cryostat shell limiting convection. Finally, L is about a few centimeters. Therefore, we are in the case where Bi is very small and the thermally thin system model is valid. The response time was found to be 63 s. In the model 340 from LakeShore the integral term is derived by dividing 1000 by the response time in seconds. We adjusted the proportional term at 600 by trial and error, and we left the derivative term at zero to achieve a good stability.

Fig. 2 shows the evolution of the system free of any regulation during 30 min, at atmospheric pressure, before wholly reaching its temperature equilibrium. There is a temperature drift of 20 $\mu\mathrm{K\,s}^{-1}$, related to the very long response time. We estimate the temperature instabilities of the free system by recording the true temperature curve and subtracting the mean value. We determined the instabilities as about ± 0.30 mK for a 1 min period.

Fig. 3 shows temperature stability during regulation at a temperature of 10 K above the low limit temperature. The graph represents the temperature recorded by the two platinum sensors, A and B. The A sensor is the feedback one. The standard deviation of the A sensor signal is ± 0.15 mK on 1 min. The B sensor is free. One notes a slight drift due to the temperature inhomogeneities in the DL's holder. This drift is about 5 $\mu\mathrm{K\,s}^{-1}$, which is insignificant.

Continuous pumping above the LN_2 allows us to work below 79 K. The temperature stability is less than without pumping, this can be explained by a non-constant pumping rate. Fig. 4 shows a record of the temperature during a 67.5 K regulation over a 100 min period. The standard deviation is ± 0.6 mK over 1 min.

3.2. Current source

Just as for the temperature, the current stability should be of high quality to reduce the DL emission linewidth. We tested two current sources by

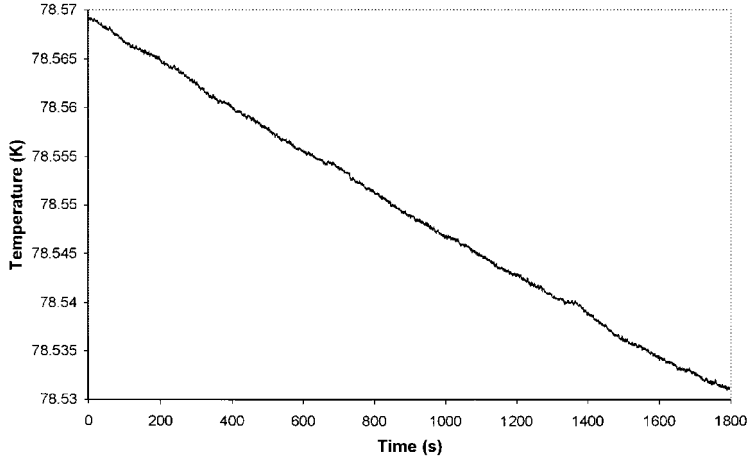

Fig. 2. Evolution of DL temperature without regulation.

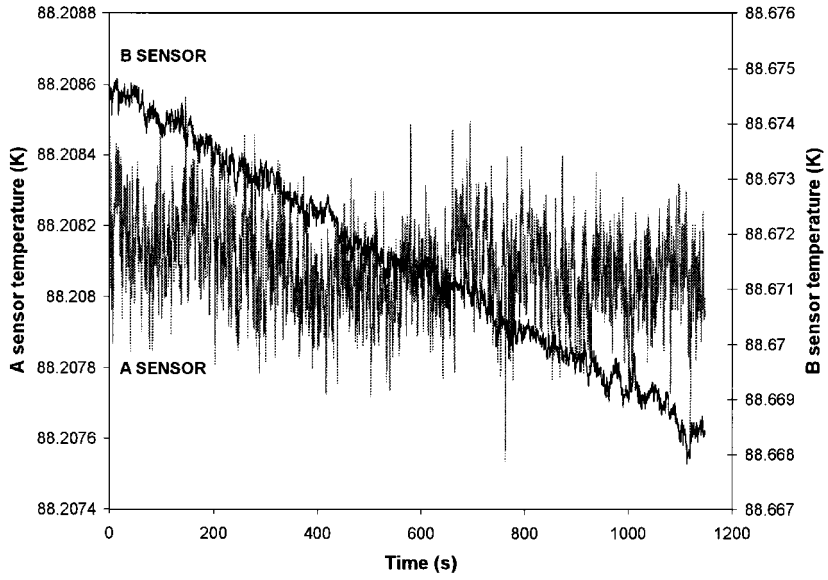

Fig. 3. Evolution of the two sensors temperature during a regulation. A sensor is the feedback one.

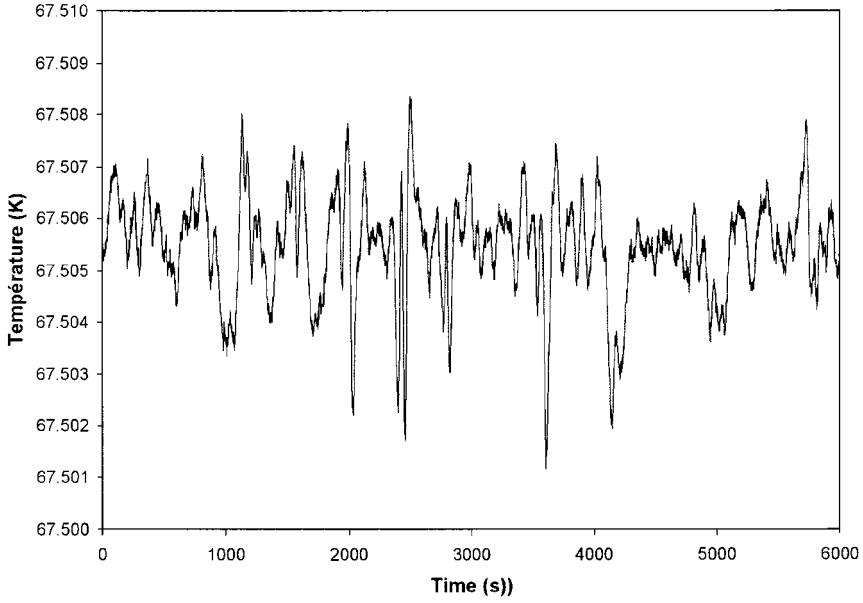

Fig. 4. Evolution of the DL temperature during a regulation with pumping above LN_2.

measuring their instabilities levels. The first one is plugged into the mains, and had a stability of ± 7 μA at 100 mA. The second one can operate directly from the mains and also from a battery. Its stability is ± 2 μA at 100 mA. Both of them are equipped with an EXT connector which allows the generation of a current ramp via an external digital system, but the first source introduced severe noise in

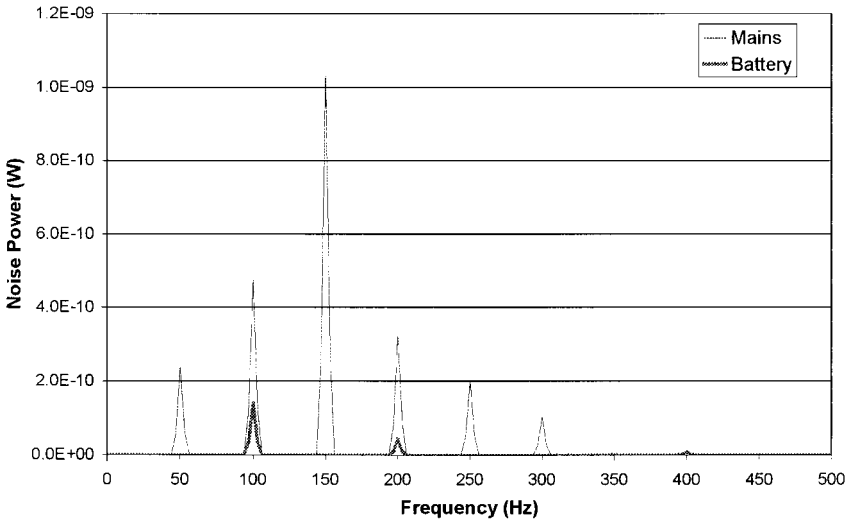

Fig. 5. Noise spectrum of the current source plugged into the mains and supplied by battery.

the ramp. For our experiments, we used the second, provided by ILX Lightwave (model LDX 3620).

We recorded the noise spectrum of the chosen source on a spectral range of 40 kHz for the two operating modes. Fig. 5 shows these noise spectra. The significant noise frequencies are below 500 Hz. They are due to the mains, and greatly decrease in the battery mode. It is clear that it is of particular interest to use the source in battery mode since all even harmonics of 50 Hz vanish, and odd harmonics considerably decreases but still remain. They are due to environmental EMI.

4. Experimental set up

Fig. 6 shows the relatively simple optical set up used for the spectroscopy experiments. The light emitted by the LD is collected by a 90° off axis parabolic mirror (PM) opened at $F/2$ (F= 50 mm). By selecting the position of flipping mirrors, the parallel beam can go optionally through a grating spectrometer (Czerny Turner type). This is very useful to obtain a coarse measurement of the wavelength emitted. The beam is modulated at the output of the spectrometer. We use two identical lenses L1 and L2 in a confocal arrangement to create a DL image. A chopper is placed at this point. The modulation frequency is 2800 Hz. The beam is then divided into two parts by a 25% reflection beamsplitter (BS).

The first beam goes through a confocal Fabry–Perrot (CFP) designed and built in the laboratory [4]. The mirrors are ZnSe parallel meniscus plates separated by 250 mm. The concave meniscus side is dielectric coated, the reflectivity of this coating is 89% at our working wavelength. The meniscus convex side is antireflection coated. The surface figure of the mirrors is about $\lambda/70$ at 8.5 μm. After the radiation traverses the CFP, it is detected by a LN_2 cooled photoconductive HgCdTe. The CFP is used as a relative frequency reference, its free spectral range (FSR) is 10^{-2} cm^{-1}. Usually the etalon used is a simple plan Fabry–Perrot like a germanium plate with a low finesse. But, a high finesse apparatus is very helpful. Indeed, the fringes' finesse permits the evaluation of the apparatus linewidth function [4]. Moreover the single mode emission of the DL is immediately checked by the fringes' appearance.

The other part of the beam goes through a BaF_2 windowed 21 cm length cell filled with 3 Torr of SO_2. The signal is then measured by a detector similar to the first one.

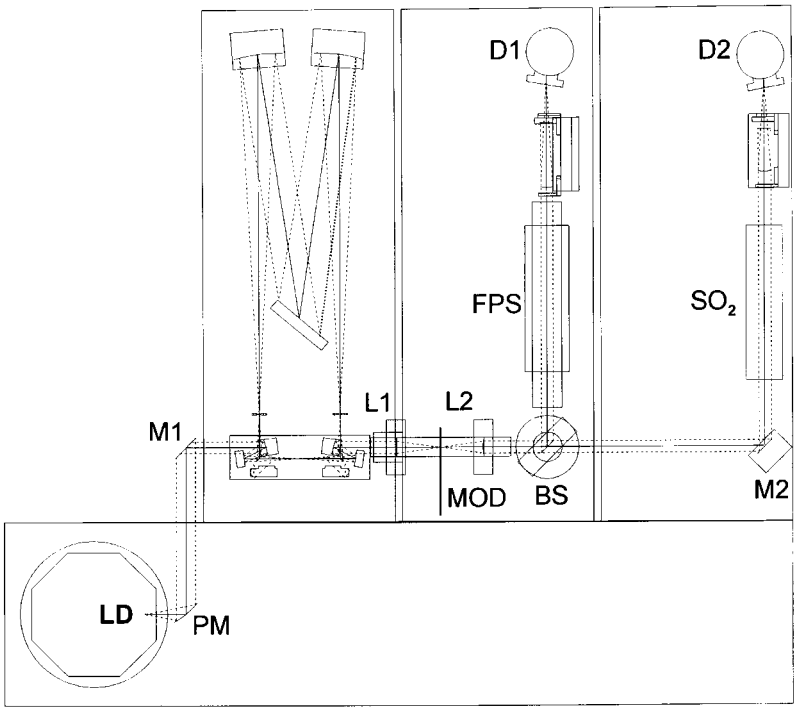

Fig. 6. Experimental set-up for absorption spectroscopy experiments.

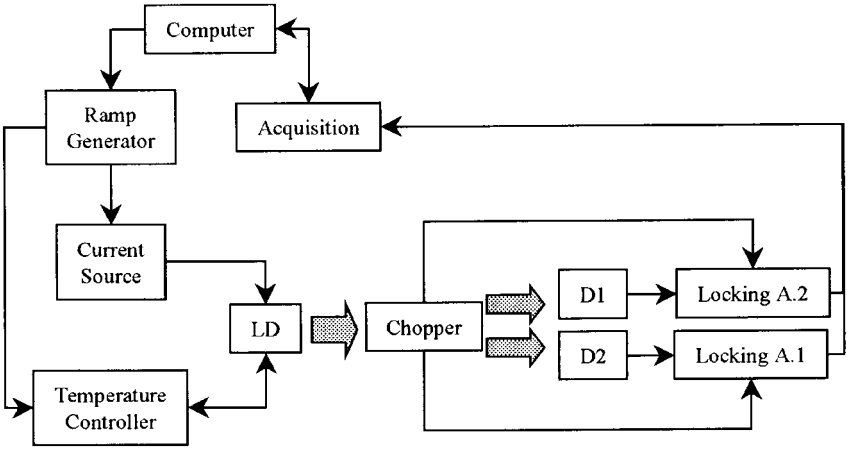

Fig. 7. Block diagram of the whole system.

As shown in Fig. 7, detected signals are sent to two lock-in amplifiers with a 3 ms time constant. The signal is recorded by a numerical acquisition system (100 measurements per second, digital integration time of 10 ms). The spectrum recording time is 40 s.

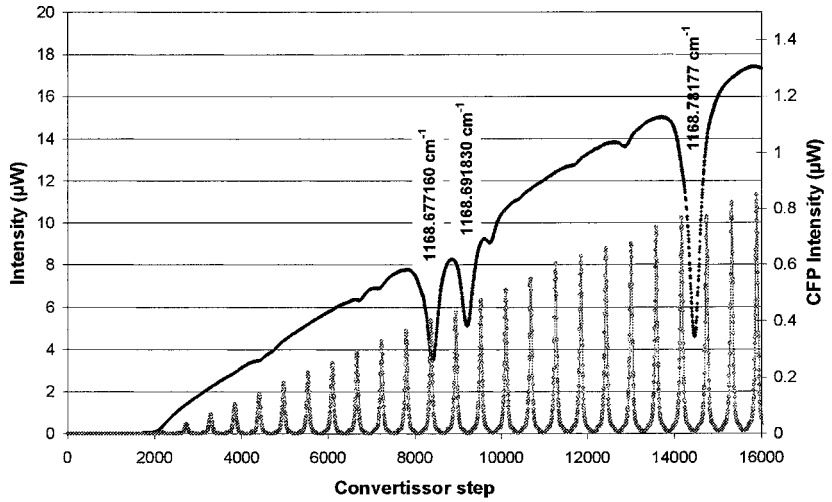

Fig. 8. SO_2 spectrum recorded by current tuning.

5. Results and discussion

Spectroscopy experiments were made in the 1168–1169 cm^{-1} (v_1 vibration) region of SO_2 absorption.

5.1. Temperature fixed, current tuning

We first record a spectrum in the classical way. The temperature was fixed and a current ramp is used for the wavelength tuning of the DL. This record is presented in Fig. 8.

For this record, the temperature was fixed at 68.5 K (pumping above LN_2). As we can see, the DL operated near its emission threshold (threshold current $I_{th} = 80$ mA). The amplitude of the current ramp was 16.5 mA. As the DL noise is lower during a single mode emission, our aim is to work under such a condition, and we usually observed that the threshold mode is single.

With such a spectrum, the absolute frequency scale can be determined. By comparing the experimental spectrum with a synthetic one, calculated from Hitran's data [5], the spectral region can be precisely recognized. Thus, for this DL, and for theses working conditions, the current tuning rate can be calculated. One finds

$$\frac{\Delta\sigma}{\Delta i} = 0.002 \text{ cm}^{-1}(\text{mA})^{-1}.$$

Knowing this current tuning rate, and knowing the current instabilities (±2 μA at 100 mA), one can estimate the emission linewidth contribution due a non-ideal current source:

$$\Delta\sigma_i = 4 \times 10^{-6} \text{ cm}^{-1}.$$

We will see that this contribution is negligible compared to temperature instabilities.

Since the DL operated at its threshold for recording this spectrum, the positive slope $dP/d\sigma$ is high (where P is the power emitted). The CFP finesse (FSR/FWHM) is 8.

5.2. Current fixed, temperature tuning

Now, we present the same spectrum recorded by temperature tuning. The digital temperature controller is able to deliver a temperature ramp of a given slope chosen by the user. Fig. 9 shows such a ramp, the slope is 0.5 K min^{-1}. On the same graph, we plot temperature instabilities during this ramp. The standard deviation of temperature instabilities, once we have removed the ramp, is about ±0.2 mK.

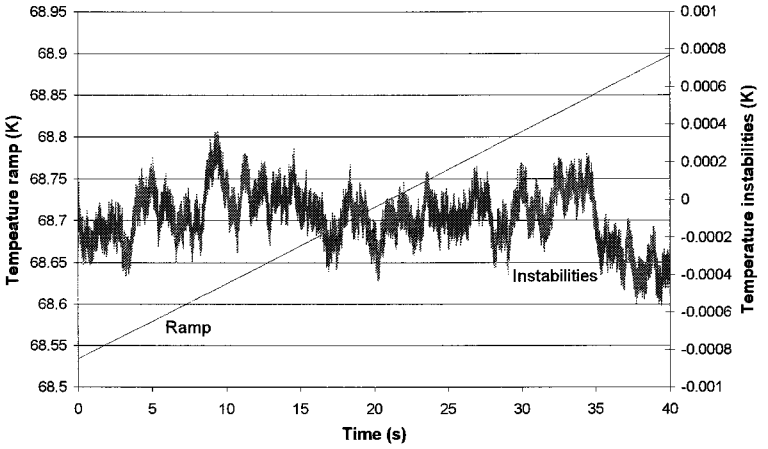

Fig. 9. Record of a temperature ramp and its associated instabilities.

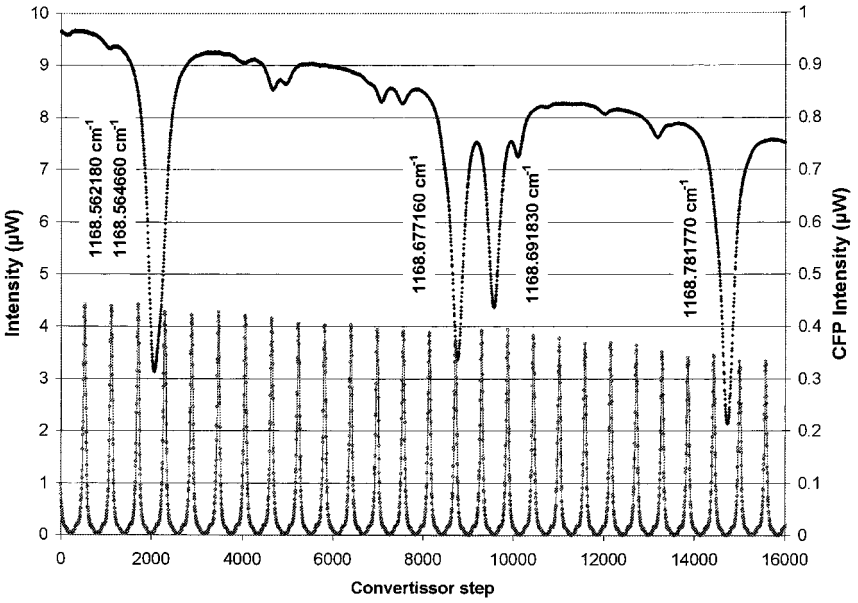

Fig. 10. SO_2 spectrum by temperature tunning.

The current is fixed at such a value that the emitted mode was the threshold one, that is to say $I = 1.1I_{\text{th}}$. Then a temperature ramp of 0.5 K min^{-1} is applied. Fig. 10 shows a record under these conditions. One can note that the exploitable spectrum region is wider since there is no threshold effect, and the negative quantity $\mathrm{d}P/\mathrm{d}\sigma$ is weak. One can compute the temperature tuning rate

$$\frac{\Delta\sigma}{\Delta T} = 0.00077 \text{ cm}^{-1}(\text{mK})^{-1}.$$

Just as for the current, we can now estimate the linewidth contribution due to temperature instabilities:

$$\Delta\sigma_T = 1.5 \times 10^{-4} \text{ cm}^{-1}.$$

The CFP finesse is 8.

To tune the DL frequency, the temperature ramp appeared to be more efficient, and is the way to obtain the largest single mode frequency range.

The first advantage of using temperature ramp is qualitative. When the DL is at a fixed temperature set point, a current ramp involves both current and temperature variation. Temperature variation due to the varying heating power of RI^2 (R is the ohmic resistance of the DL) cannot be avoided. When the DL is at a fixed current set point, the power dissipation is constant and so the frequency tuning is only made by the variation of temperature. The tuning is therefore very predictable.

Wavelength tuning is due to two phenomena. Firstly a tuning that we will call coarse which is linked to the maximum gain curve of the amplifier medium (active zone). The other, the fine one, is related to the index variation of the DL Fabry–Perrot cavity.

The gain curve of the amplifier medium is affected by two parameters: the injection current and the temperature. The way they modify the gain curve is different.

An injection of carriers in a biased p–n junction modifies the quasi Fermi energy levels of the conduction and valence bands. Thus the energy of the most probable radiative transition changes. Moreover (Fig. 11 shows a calculation on the gain curve) when the injection current increases, the gain coefficient increases too [6] (so the power emitted if the emission is single mode and if there is no saturation effect) and the gain curve broads. This explains the fact that $dP/d\sigma$ is positive and rather high during a current ramp. The broadening of the gain curve also explains the fact that a multimode emission is more likely to appear. The quantity $d\sigma/di$ is positive.

Temperature operates differently. Of course it has an effect on the energy distribution of carriers. But, the most important contribution is the gap energy dependence with temperature. For our lead salt diodes, the active zone is in PbSe. Ref. [7] gives this material's energy gap dependence with temperature. Fig. 12 shows a calculation of the gain curve for different temperatures. We observe a translation of the gain curve, without broadening which favors single mode emission. The maximum of the gain curve is slowly decreasing. This is consistent with the observed negative and weak $dP/d\sigma$ during a temperature ramp. The quantity $d\sigma/dT$ is still positive.

Understanding the variation of gain curve with current and temperature is helpful to understand the starting mode or mode hoppings. But, the fine tuning of the wavelength in a given single mode zone (wider single mode zones are about 1 cm^{-1}) is

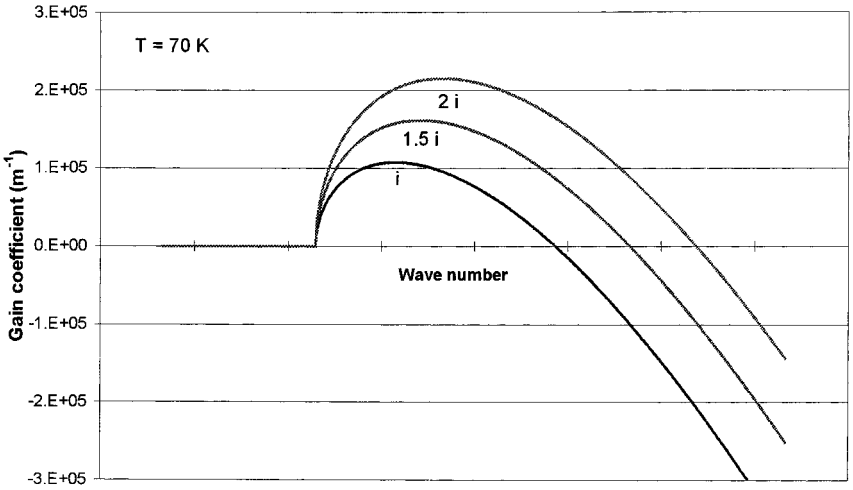

Fig. 11. Evolution of the active zone gain curve for three different injection currents.

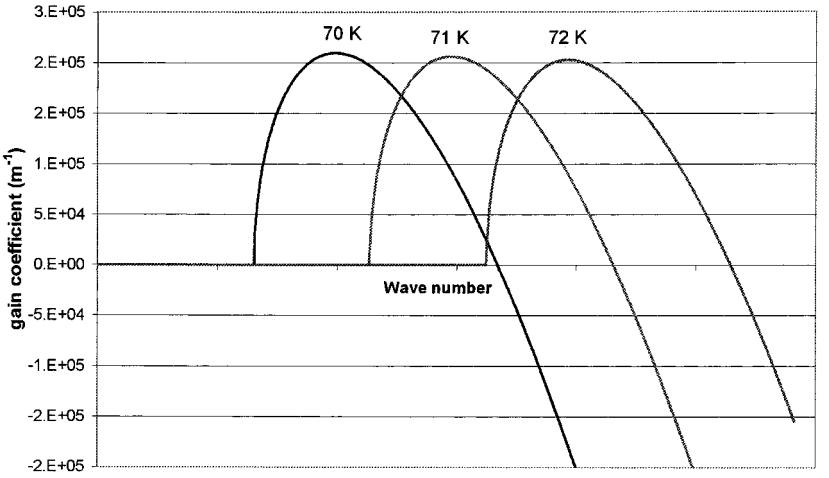

Fig. 12. Evolution of the active zone gain curve for three different temperatures.

due to the refractive index changes of the active zone. In the laser cavity, the emitted mode is a resonant one. The wavelength should satisfy

$$q\lambda = 2n(i,T)L, \tag{5.1}$$

where q is an integer, λ, the wavelength, L, the geometric length of the cavity, and n, the refractive index depending of current and temperature.

In fact, it is very difficult to dissociate the tuning mechanisms since they are related by the Kramers–Kronig relations.

The experimental linewidth of the apparatus function can be determined from the known emission linewidth broadening due to temperature and current drifts. We have

$$I_{\mathrm{M}} \propto f_{\mathrm{DL}} \otimes f_{\mathrm{CFP}} \tag{5.2}$$

with

$$f_{\mathrm{CFP}} = \frac{1}{1+\rho^2}\,\frac{1}{1+\left(\frac{2\rho}{1-\rho^2}\right)^2 \sin^2(4\pi \mathrm{d}\sigma)}, \tag{5.3}$$

where I_{M} in the measured CFP signal (function of σ), f_{DL} is the DL emission spectrum, that is to say the apparatus function (also a function of σ), f_{CFP} is the Airy function of the Fabry–Perrot, ρ, the reflection coefficient of CFP mirrors, d, the CFP cavity length, σ, the wave number, and $\otimes$ denotes convolution.

Supposing that the apparatus function f_{DL} is gaussian shaped, we are able to compute the resultant intensity of the CFP signal. By comparison with the experimental record, we evaluate the linewidth of f_{DL}. With this method, it appears that the apparatus function linewidth is around 0.6×10^{-3} cm^{-1} (18 MHz). This is the FWHM of the DL emission spectrum that we call $\Delta\sigma_{\mathrm{DL}}$. One can write

$$\Delta\sigma_{\mathrm{DL}} = \sqrt{\Delta\sigma_{\mathrm{nat}}^2 + \Delta\sigma_i^2 + \Delta\sigma_T^2} \tag{5.4}$$

with $\Delta\sigma_{\mathrm{nat}}$ the natural DL emission linewidth, $\Delta\sigma_i = 4 \times 10^{-6}$ cm^{-1} and $\Delta\sigma_T = 1.5 \times 10^{-4}$ cm^{-1} the current and temperature contribution to the DL emission linewidth. Whatever the tuning mode, the current and the temperature instabilities are the same. Thus, we determined a natural emission linewidth of 10 MHz.

6. Conclusion

Our infrared DL source gives high quality spectra. Whatever the tuning mode we chose, temperature and current instabilities add their contribution to the linewidth. The limiting feature is often temperature stability. Here we reach ±0.00015 K.

We use a temperature ramp to tune the frequency DL. This technique is very efficient. The single mode emission range is wider in frequency and permits a quick observation of single mode regions. We deduce an estimate of our DL's emission linewidth of 10 MHz.

Acknowledgements

We are very grateful to Messrs. P. Von Der Heyden, G. Jacquelet and J. Poncelet for the mechanical realization of our cryostat. We want to greatly thank Mr. X. Thomas for the realization of the acquisition system and software, and Mr. A. Luna for its constant availability.

References

[1] R.S. Eng, J.F. Butler, K.J. Linden, Optical Engng. 19 (6) (1980) 945.
[2] M. Ohtsu, Y. Teramachi, IEEE J. Quant. Elec. 25 (1) (1989) 31.
[3] J. Reid, T. Cassidy, R.T. Menzies, Appl. Opt. 21 (21) (1982) 3961.
[4] M.R. DeBacker, B. Parvitte, X. Thomas, V. Zeninari, D. Courtois, J. Quant. Spectrosc. Radiat. Transfer 59 (1998) 3–5.
[5] Hitran Database (1996).
[6] G.P. Agrawal, N.K. Dutta, Long Wavelength Semiconductors Lasers, Van Nostrand Reinhold, New York.
[7] I. Melngailis, A. Mooradian, Laser Applications to Optics and Spectroscopy, in: S.F. Jacobs, M. Sargent III, J.F. Scott, M.O. Scully (Eds.), Addison-Wesley, Reading, 1975.